Surface Science 605 (2011) 81–88

Contents lists available at ScienceDirect

Surface Science

journal homepage: www.elsevier.com/ locate/susc

Interaction of NO with Au nanoparticles supported on (100) terraces and topological defects of MgO

Silvia A. Fuente [a,b], Ricardo M. Ferullo [a,b,*], Nicolás F. Domancich [a], Norberto J. Castellani [a]

[a] Grupo de Materiales y Sistemas Catalíticos, Departamento de Física, Universidad Nacional del Sur, Av. Alem 1253, 8000 Bahía Blanca, Argentina
[b] Departamento de Química, Universidad Nacional del Sur, Av. Alem 1253, 8000 Bahía Blanca, Argentina

ARTICLE INFO

Article history:
Received 16 July 2010
Accepted 1 October 2010
Available online 8 October 2010

Keywords:
Nitric oxide
Au/MgO
Model catalysts
NO adsorption
DFT
Cluster model

ABSTRACT

The adsorption of nitric oxide (NO) on Au_n (n = 1–3) particles deposited on anionic (O^{2-}) sites of MgO has been studied using the DFT (Density Functional Theory) approach. The regular O^{2-} sites of MgO(100) and the sites in edge and corner topological defects with high symmetry of MgO were considered. The adhesion energy of Au_n to MgO is larger for Au_2 and Au_3 due to higher polarization effects. On the other hand, the interaction strength of NO with supported Au_n particles depends mainly on the electronic configuration (open or closed shell) of the particle; the Au particles with odd number of atoms show larger NO binding energies. A comparison was performed with the reactivity of free Au_n particles. From this, it is possible to conclude that the support enhances the NO–Au_n bonding strength for the monomer, weakens this interaction in the case of the dimer, and does not have an effect in the trimers. Besides, the NO–Au_n bonding is essentially insensitive to the coordination of the anionic site where the Au_n particle is linked. A large red-shift of the N–O stretching frequency was obtained, particularly for the Au particles with odd number of atoms, due to a negative charge transfer from Au to NO.

1. Introduction

Supported Au nanoparticles present an extraordinary activity to catalyze different reactions at low operating temperatures, such as the oxidation of CO, the partial oxidation of hydrocarbons and the reduction of NO_x [1]. TiO_2 have been used as the typical support for Au particles, but other oxides like MgO, SiO_2 and Al_2O_3 were also considered [1–4].

Nitrogen oxides are air-pollutants produced by combustion engines. Therefore, the necessity to develop efficient catalytic converters for the post-processing of the exhaust gases has stimulated extensive investigations of the adsorption and decomposition of NO_x molecules on the surfaces of metallic catalysts (for reviews see, for example, Refs. [5,6]).

In particular, the catalytic reduction of nitrogen oxides towards N_2 and O_2 is one of the most important reactions that takes place in the three-way catalysts [7,8]. A highly practical and suitable method to remove NO_x seems to be the catalytic reduction using compounds such as CO, hydrogen and hydrocarbons contained in exhaust gases. Ueda and Haruta [4] found that Au catalysts supported in a variety of metallic oxides show a great catalytic activity in the reduction of NO with hydrocarbons such as propene, propane, ethene and ethane.

As one of the key factors to understand certain catalytic mechanisms, the adsorption of NO molecules on unsupported Au particles has been experimentally studied. For example, Citra et al. [9] analyzed the reaction of Au clusters with NO at very low temperatures producing neutral complexes like AuNO and $Au(NO)_2$ as principal products. On the other hand, Ding et al. [10] performed theoretical studies for the adsorption of NO on Au clusters with 1 to 6 atoms in neutral as well as in positively and negatively charged states. They found that all these Au aggregates are able to adsorb NO with greater adsorption energies for cationic clusters.

MgO is usually used as a model support due to its simple crystal structure and because it presents different types of defects which are relatively easy to be included in the simulations. The deposition of Au aggregates on the MgO(100) surface has been deeply studied using the DFT approach [11–19]. Most of the theoretical works dealing with the adsorptive and catalytic properties of Au/MgO have used CO as probe molecule. Basic aspects, such as the CO-induced modification of the Au–MgO interface [20], the vibrational properties of CO adsorbed on Au_1/MgO [21,22], and the paramagnetic behavior of CO/Au/MgO [23] were investigated. Besides, it was observed that three-dimensional and two-dimensional nanoclusters deposited on MgO [24–26] and MgO/Mo [27], respectively, show a remarkable activity for CO oxidation.

Among the very small Au particles, Au_1 and Au_3 present the highest NO adsorption energies [10]. Therefore, the study of the NO adsorption capability of these tiny particles in a supported state could be of great interest. In a previous work [28] we have presented a

* Corresponding author. Grupo de Materiales y Sistemas Catalíticos, Departamento de Física, Universidad Nacional del Sur, Av. Alem 1253, 8000 Bahía Blanca, Argentina. Tel.: +54 291 4595141; fax: +54 291 4595142.
E-mail address: caferull@criba.edu.ar (R.M. Ferullo).

0039-6028/$ – see front matter © 2010 Elsevier B.V. All rights reserved.
doi:10.1016/j.susc.2010.10.003

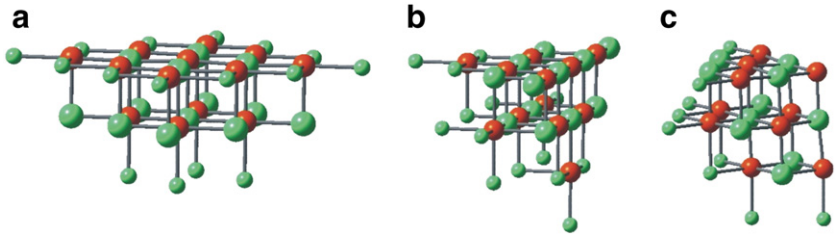

Fig. 1. a) $Mg_{13}O_{13}$(Mg-ECP)$_{16}$ cluster used for modeling the MgO(100) surface. b) $Mg_{12}O_{12}$(Mg-ECP)$_{14}$ cluster used for modeling the edge topological defect of MgO due to the intersection of two [100] and [010] oriented planes. c) $Mg_{10}O_{10}$(Mg-ECP)$_9$ cluster used for modeling the corner topological defect of MgO due to the intersection of three [100], [010] and [001] oriented planes. Red spheres: O. Green spheres: Mg. Small green spheres: Mg-ECPs. Point charges are not shown.

molecular orbital study on the NO interaction with Au monomers and dimers anchored on the MgO(100) surface. We found that when the Au atom is adsorbed on an anionic site it essentially retains its spin and for this reason it can couple efficiently with NO (a radical); conversely, when the Au atom is deposited on an O-vacancy the Au–NO bond is relatively weak because of the partial spin delocalization toward the cavity. In the present paper, we extend the study by considering O^{2-} sites at edge and corner topological defects of MgO and also including the gold trimer.

This work is divided in two sections: 1) adhesion of Au particles (1–3 atoms) in a O^{2-} site of the MgO(100) surface (terrace site) as well as on O^{2-} sites at topological defects (edge and corner sites); and 2) adsorption of NO on Au particles supported on the same sites of MgO.

2. Computational details

Density Functional Theory (DFT) molecular orbital calculations were performed using the gradient corrected Becke's three parameters hybrid exchange functional in combination with the correlation functional of Lee, Yang and Parr (B3LYP) [29]. All the calculations have been carried out using the Gaussian-03 program package [30]. The terrace site at MgO (100) surface was represented by a $Mg_{13}O_{13}$ cluster consisting of two layers (first layer: Mg_4O_9; second layer: Mg_9O_4). To take into account the Madelung field due to the rest of the extended surface, the cluster was embedded in an array of ± 2 point charges. Besides, the positive point charges at the interface between the cluster region and the region of point charges were replaced by effective core potentials (ECP) corresponding to the Mg^{2+} cation to account for its finite size and to avoid spurious charge polarization. The corresponding $Mg_{13}O_{13}$(Mg-ECP)$_{16}$ cluster is represented in Fig. 1a. This embedding technique was used previously for the study of both bulk and surface properties giving results which are in good agreement with those obtained by periodic calculations [21,31–33]. For the topological defects, a similar modeling was used resulting in the following clusters: $Mg_{12}O_{12}$(Mg-ECP)$_{14}$ (edge sites) and $Mg_{10}O_{10}$(Mg-ECP)$_9$ (corner sites) (Fig. 1b and c, respectively).

While the atomic orbitals of the oxygen ion acting as the adsorption site and its nearest four O neighbors (three for corner site) were described by the 6–31+G(d) basis set, those of the exposed Mg ions (four for terrace and edge sites, three for corner site) directly bonded with the O adsorption site were expressed using the 6–31G (d) basis set; for the rest of the Mg and O ions of the cluster, the 6–31G basis set was used. The 6–31+G(d) basis set was employed for the

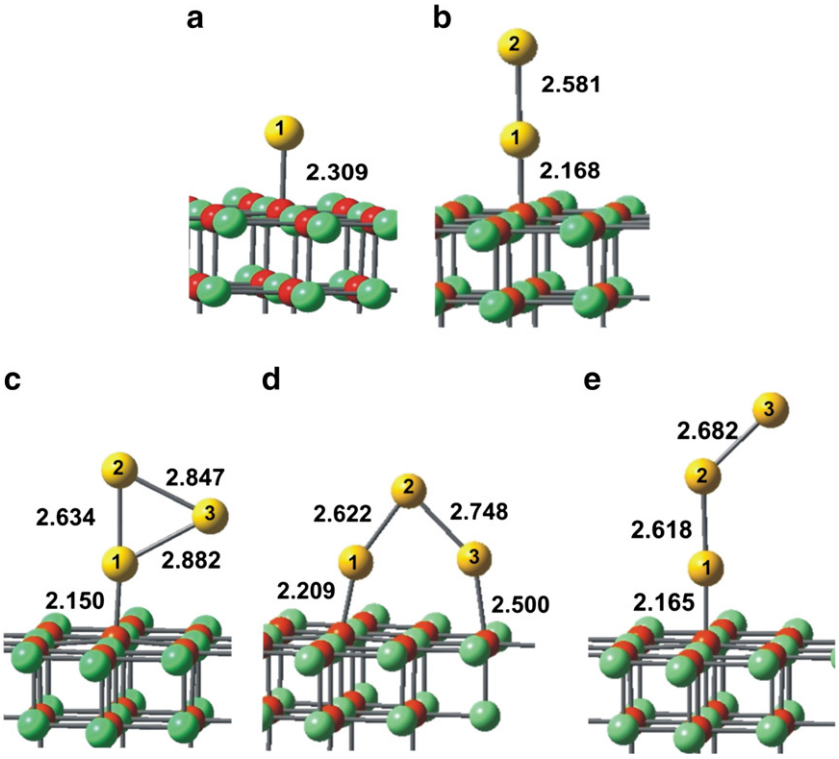

Fig. 2. Schematic representations of Au_n (n = 1–3) clusters deposited on a O^{2-} site of the MgO(100) surface. a) Monomer; b) dimer; and c)–e) trimers. Red spheres: O. Green spheres: Mg (including Mg-ECPs). Yellow spheres: Au.

Table 1
Main energetic and electronic population parameters for Au particles deposited on anionic sites of MgO(100) (terrace).

	Au_1/MgO	Au_2/MgO	Au_3/MgO		
			Fig. 2c	Fig. 2d	Fig. 2e
E_{adh} (eV)	0.73	1.34	1.36	1.30	1.32
E_{nucl}	–	2.56	0.80	0.77	0.79
q[Au(1)] (*e*)	−0.13	0.14	0.23	0.12	0.14
q[Au(2)]	–	−0.28	−0.14	−0.11	−0.14
q[Au(3)]	–	–	−0.23	−0.23	−0.15
q(Au_n)	−0.13	−0.14	−0.14	−0.22	−0.15
SD[Au(1)]	0.76	–	0.00	0.23	0.23
SD[Au(2)]	–	–	0.32	0.00	0.00
SD[Au(3)]	–	–	0.70	0.55	0.59

atoms of the NO molecule. On the other hand, for Au, the Los Alamos basis set was used (LANL2DZ), which describes the 19 valence 5*s*25*p*65*d*106*s*1 electrons with a [5*s*,6*p*,4*d*/3*s*,3*p*,2*d*] basis set and the one-electron interaction with the 60 core electrons with a relativistic pseudopotential [34,35]. In the geometrical optimization procedure, the atomic coordinates of the adsorbate (Au_n or NO/Au_n) were fully optimized, together with the coordinates of the central oxygen anion (the adsorption site) and the four surface Mg cations directly bonded to it (three for corner site). Only the adsorption on anionic sites was studied because it is well established that these are the preferred adsorption sites for transition metals [36].

We define the adhesion energy (E_{adh}) of the Au_n particle on MgO as follows:

$$E_{adh} = -[E(Au_n/MgO) - E(MgO) - E(Au_n)]; \quad n = 1,2,3. \tag{1}$$

The nucleation energy (E_{nucl}) is an important parameter to study the atom-by-atom growth of a particle from atoms in the gas phase. It is defined as the energy associated with the formation of a Au particle when an atom of the gaseous phase bonds with a pre-adsorbed metallic particle:

$$E_{nucl} = -[E(Au_n/MgO) - E(Au_{n-1}/MgO) - E(Au_1)]; \quad n = 2,3. \tag{2}$$

On the other hand, we define the binding energy (E_B) of NO molecule on Au/MgO as

$$E_B = -[E(NO/Au_n/MgO) - E(Au_n/MgO) - E(NO)]; \quad n = 1,2,3. \tag{3}$$

Positive values correspond to exothermic processes. The basis set superposition error (BSSE) was corrected following the counter-poise procedure [37]. We have analyzed the cluster size dependence of the binding energies in a previous work [21].

N–O vibrational frequencies were computed by determining the second derivatives of the energy with respect to the Cartesian nuclear coordinates and then transforming to mass-weighted coordinates. The frequency values were scaled according to the factor of 0.9465, calculated as the ratio between the empirical and the calculated frequency values for the isolated NO molecule (1876/1982).

The net atomic charges and the spin density (SD) were calculated following the Natural Bond Orbital (NBO) method [38]. This approach for the charge partitioning was recently applied to analyze the interaction of CO and NO with coinage metals [9,10,39,40]. The direction of charge transfer predicted from NBO atomic charge values is consistent with calculated core level shifts [21] and with dipole moment changes [41]. The SD values obtained with the NBO method are only slightly different than those obtained with the Mulliken population analysis used in a previous work [28].

3. Results and discussion

3.1. Adhesion of Au_n at (100) terraces and topological defects of MgO

In Fig. 2 the optimized geometries of Au supported particles anchored on terrace sites of MgO(100) are shown. In Table 1, the corresponding values of adhesion and nucleation energies, atomic charges and spin densities have been summarized. For dimers and trimers, the different Au atoms are identified by numbers: Au(1), Au (2) and Au(3) (also in Fig. 2). For Au_2, different initial geometries converge to the same structure, namely, that perpendicular to the surface (Fig. 2b). On the other hand, for Au_3, three different geometries were found. The most stable configuration is a nearly isosceles triangle with its shortest side perpendicular to the surface (Fig. 2c). In the second geometry, the trimer overturns towards the surface, anchoring to two O^{2-} sites (Fig. 2d); in the third case, the trimer adopts a quasi-linear perpendicular orientation (Fig. 2e). The three geometries have very similar adhesion energies.

It is clear from Table 1 that the gold adhesion to the oxide surface is more favorable for Au_2 and Au_3 than for Au atom. The nucleation energy (E_{nucl}) value for Au_2, i.e., the energy implied in linking one Au atom to a Au atom previously adsorbed, is much more significant than the binding energy of an isolated Au to a O^{2-} site (2.56 eV vs. 0.73 eV). In free molecule condition, the calculated nucleation energy (in this case, the dimerization energy) is 1.86 eV; then, the Au–Au bond is favored in 0.7 eV owing to the effect of the support. A very similar value was reported by Del Vitto et al. [11] (0.6 eV) using periodic supercells. In the case of trimers, the nucleation energy is much lower than that for the dimer (around 0.8 eV).

Analyzing the atomic charges, we notice that when a Au atom interacts with MgO, a very small electronic transfer is produced from the oxide to the metallic atom (0.13*e*). Results from EPR (Electron Paramagnetic Resonance) spectroscopy of Au atoms deposited on MgO(100) suggest that single gold atoms are essentially neutral [42]. On the other hand, the analysis of the electronic charge distribution reported in Refs. [11] and [28] shows an important polarization

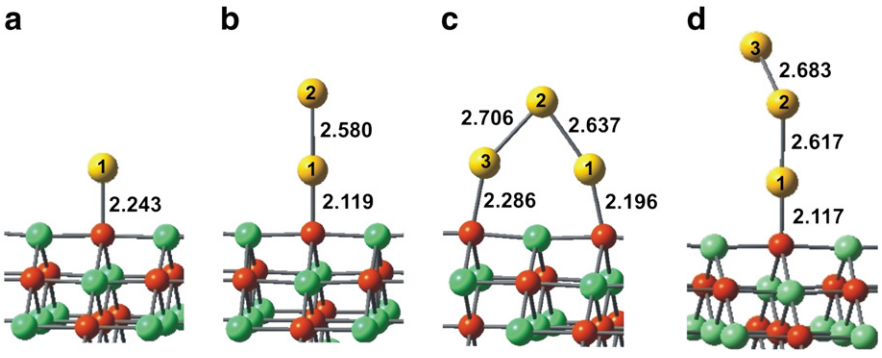

Fig. 3. Schematic representations of Au_n (n = 1–3) clusters deposited on a O^{2-} site of the edge topological defect of MgO. a) Monomer; b) dimer; and c)–d) trimers. For the references to colors, see the figure legends of Fig. 2.

Table 2
Main energetic and electronic population parameters for Au particles deposited on anionic sites at the edge defect.

	Au_1/MgO	Au_2/MgO	Au_3/MgO	
			Fig. 3c	Fig. 3d
E_{adh} (eV)	0.90	1.55	1.75	1.51
E_{nucl}	–	2.40	1.00	0.77
q[Au(1)] (*e*)	−0.14	0.15	0.04	0.13
q[Au(2)]	–	−0.29	−0.11	−0.15
q[Au(3)]	–	–	−0.16	−0.15
q(Au_n)	−0.14	−0.14	−0.23	−0.17
SD[Au(1)]	0.72	–	0.23	0.13
SD[Au(2)]	–	–	0.20	0.10
SD[Au(3)]	–	–	0.47	0.60

contribution to the bond between Au and the five-coordinated oxygen anion (O_{5c}), due to the intraunit polarization of the adsorbed Au atom. For the Au_2 and Au_3 clusters, an electronic charge transfer occurs from the oxygen anion with a value similar than that for the monomer; the Au atom directly linked with the O^{2-} site becomes positively charged, whereas the others are negatively charged. Therefore, also Au_2 and Au_3 particles undergo a polarization induced by the interaction with the oxide surface.

Aside from the polarization contribution, some covalent mixing in the Au_1–O_{5c} bond was suggested by Del Vitto et al. [11]. From our study, we observe a decrease of the SD(Au) value, from 1 to 0.73, when such atom changes from being free to be anchored on a terrace site. In the last situation, the O_{5c} anion linked with Au attains a non negligible SD value, 0.24; this is compatible with the partial shearing of one fourth of an electron up (from Au) and one fourth of an electron down (from O_{5c}) in a covalent contribution to the Au–O_{5c} bond. For the Au_3/MgO system the total spin is entirely localized on the metallic particle for the nearly isosceles configuration (Fig. 2c), and it has a value of about 0.8 for the other two structures indicating some covalent mixing with the surface. For the dimer, the SD is zero because the Au_2/MgO system is a singlet in its fundamental state. On the other hand, the different reactivities of monomer and dimer to bind with an additional Au atom in the nucleation process can be explained by means of this SD distribution. While the adsorbed monomer has an open shell structure, the dimer presents a closed one; thus, the interaction is much more favored in Au_1/MgO because in this case a direct coupling between two species with unpaired electrons is produced.

In Fig. 3, the optimized geometries of Au supported particles anchored on a MgO edge are shown. This topological defect is modeled by the intersection of two [100] and [010] oriented planes. In Table 2, the main energetic and electronic population parameters corresponding to this site have been summarized. The dimer shows similar geometry as for the terrace site, perpendicular to the edge, but residing nearly in its bisecting plane (Fig. 3b). On the other hand, the trimers show only two geometric configurations that are similar to the overturned triangle and the quasi-linear trimers on terrace. Other triangle conformers were tested as starting geometries, but all of them converged to the overturned triangle, which in turns is an indication of the higher reactivity of the four-coordinated oxygen anions (O_{4c}).

The higher reactivity of O_{4c} is also evidenced in the E_{adh} values of Table 2 which are about 0.2 eV larger than on terrace. For the trimer with the overturned triangle geometry the stability difference is greater: 0.4 eV. In the same way as for terrace, an electronic charge transfer is produced from the oxygen anion to the Au particle; this charge is mainly localized on the terminal Au atoms of Au_2 and Au_3, indicating also here a metal–oxide interaction of polarization type. The spin is mainly concentrated over the Au_3 particle with a total SD value between 0.8 and 0.9. For the atomic case, the SD values are similar than for the terrace (SD(Au) = 0.72; SD(O_{4c}) = 0.24) indicating also here some covalent contribution.

Finally, the calculations corresponding to the Au supported particles anchored in a corner site of MgO are shown in Fig. 4. This site was modeled by the intersection of three [100], [010] and [001] oriented planes. From Fig. 4 and Table 3 we notice that for Au_1 and Au_2 two different geometrical configurations were obtained, with very near adhesion energies. The dimers adopt geometries where the two Au atoms and the O anion are aligned. The geometrical configurations of the trimers are similar to those on terrace. Regarding the corner reactivity, for the most stable conformers the adhesion energy is 0.2–0.3 eV larger on corner than on edge. Also in this case, for Au_2 and Au_3, the support induces an internal charge transfer to the terminal Au atoms and the spin on Au_3 is located mainly on the metal particle.

Considering the above comments about the behavior of Au particles on different anionic sites of MgO, we can conclude that in general for each type of site (terrace, edge or corner) the bond strength between the metallic particle and the anionic site of MgO follows the order: Au_3>Au_2>Au_1, though the E_{adh} difference between the dimer and the trimer is not significant (less than 0.2 eV). Moreover, for each type of particle (Au_1, Au_2 or Au_3) the bond strength follows the order: corner>edge>terrace (see Fig. 5). Considering the nucleation energy of each metallic particle, the incorporation of the second Au atom is significantly more favored than the third one, irrespective of the type of site (terrace, edge or corner).

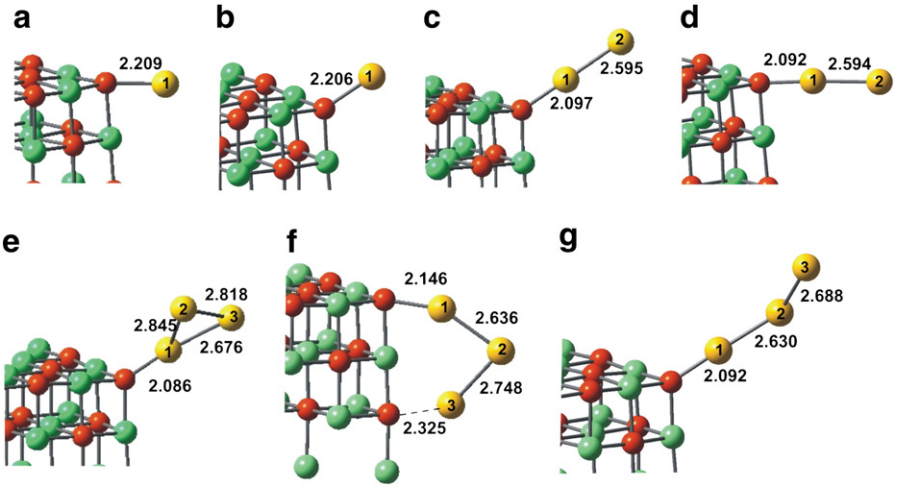

Fig. 4. Schematic representations of Au_n (n = 1–3) clusters deposited on a O^{2-} site of the corner topological defect of MgO. a–b) Monomers; c–d) dimers; and e–f) trimers. For the references to colors, see the figure legends of Fig. 2.

Table 3
Main energetic and electronic population parameters for Au particles deposited on anionic sites at the corner defect.

	Au_1/MgO		Au_2/MgO		Au_3/MgO		
	Fig. 4a	Fig. 4b	Fig. 4c	Fig. 4d	Fig. 4e	Fig. 4f	Fig. 4g
E_{adh} (eV)	1.11	1.05	1.89	1.90	2.00	2.04	1.85
E_{nucl}	–	–	2.61	2.62	0.87	0.95	0.75
q[Au(1)] (*e*)	−0.15	−0.15	0.21	0.19	0.33	0.17	0.22
q[Au(2)]	–	–	−0.37	−0.34	−0.25	−0.20	−0.19
q[Au(3)]	–	–	–	–	−0.27	−0.20	−0.21
q(Au_n)	−0.15	−0.15	−0.16	−0.15	−0.19	−0.23	−0.19
SD[Au(1)]	0.69	0.72	–	–	0.00	0.21	0.20
SD[Au(2)]	–	–	–	–	0.40	0.00	0.14
SD[Au(3)]	–	–	–	–	0.61	0.53	0.58

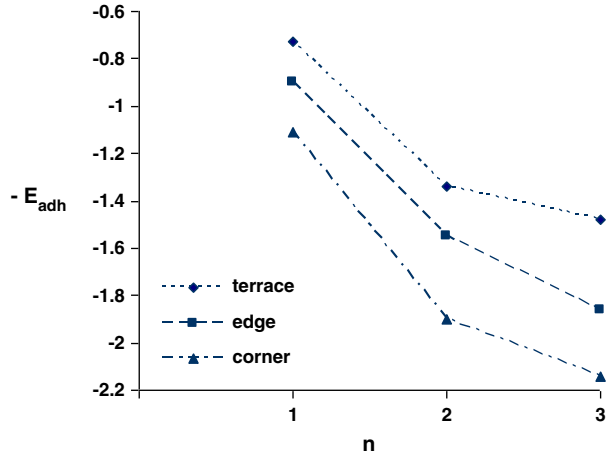

Fig. 5. Adhesion energies (E_{adh} in eV) vs. the number of Au atoms in Au_n particles deposited on terrace, edge and corner. For the trimers, only the result for the most stable structure is reported.

Taking into account the relative high mobility of Au aggregates on MgO(100) [43] it is interesting to consider the energetic changes taking place during the diffusion process from the O^{2-} site on terrace to the more reactive site at a corner defect. From our results, the energetic stabilizations for that process are: 0.4 eV for Au_1, 0.6 eV for Au_2 and 0.7 eV for Au_3. However, from previous calculations we can deduce that the corresponding stabilization is much higher for the diffusion toward another type of surface defects, namely the O-vacancies of MgO, in particular those produced by removing a neutral O atom. For example, Au_1 stabilizes in the range of 2.2–2.4 eV for the diffusion from O^{2-} on terrace to an O-vacancy on terrace or topological defects [21]. For Au_2 a similar value was obtained considering the diffusion from O^{2-} to an O-vacancy both on terrace [28]. Hence, although the energetic stabilization on topological defects is not negligible, in defect-rich MgO surfaces it would be expected that O-vacancies, rather than O^{2-} centers at topological defects, could act as efficient traps for the diffusing Au particles.

3.2. Adsorption of NO on Au_n (n = 1, 2, 3) supported in anionic sites (O^{2-}) of MgO

In Fig. 6, the optimized geometries of NO adsorption on Au_n/MgO (terrace sites) are shown, and in Table 4 the corresponding values of binding energies, atomic charges and spin densities. The N–O stretching frequencies were also included. In all the cases the NO molecule adopts a tilted orientation with respect to the Au atom which it is bonded; the Au–N–O angle is 116.7° for the adsorbed monomer, and 126.8° for the dimer (Fig. 6a and b). Regarding the trimer, two structures were obtained: one locating the NO molecule over Au(2) of Fig. 2c and the other over Au(3) of Fig. 2d as starting geometries. The adsorption over the quasi-lineal Au_3 structure was not considered. In both cases, the NO molecule tilts towards the MgO surface, and a bond between the O atom of NO and a surface Mg^{2+} cation is produced. The final optimized geometries correspond to Au–N–O angles of about 120° (Fig. 6c and d). In both configurations the O atom of NO acquires a considerable negative charge, −0.3*e*, which allows an electrostatic interaction with a surface Mg^{2+} cation at the border of the cluster. Actually, it is one of the ECPs at the interface with the embedding of point charges. In order to test if this interaction is well represented by this cluster, the calculation was repeated with a larger cluster, $Mg_{25}O_{25}(Mg\text{-}ECP)_{25}$, in which this Mg-ECP was replaced by a Mg atom and the entire cluster was enlarged accordingly. This was performed for the configuration of Fig. 6d. We observed that the Au–Au, Au–NO and N–O distances were very similar for the two clusters. On the other hand, the calculated value of E_B for NO is only 0.1 eV higher than the value with the smaller cluster. Thus, the $Mg_{13}O_{13}(ECP\text{-}Mg)_{16}$ cluster seems to represent in a reasonable way the interaction with the adsorbate.

In Fig. 7 and Table 5, the main results corresponding to the NO adsorption on Au_n/MgO for the edge defect are shown. As on terrace, only one configuration is possible for monomer and dimer; on the other hand, for the trimer two different geometrical configurations were found, as shown in Fig. 7c and d. The N–O bond tilts with a Au–N–O angle of about 120° in all the cases. In the first configuration of trimers, shown in Fig. 7c, the NO molecule links to Au(1) producing a very important weakening of the Au(1)–Au(2) bond which becomes about 0.6 Å longer with respect to the bond in the adsorbed trimer without NO. This configuration can be considered as formed by two independent adsorbed species, Au_2 and Au_1NO; indeed, the Au–Au distance (2.587 Å) is very similar to that of Au_2 in the edge (2.580 Å, see Fig. 3b), and the Au_1NO species is very similar to the situation

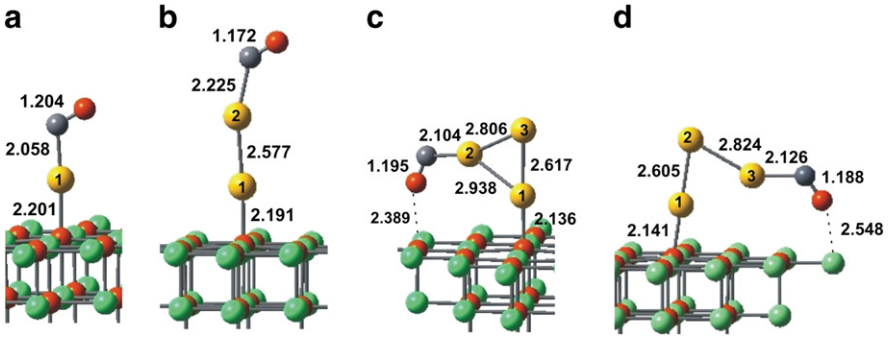

Fig. 6. Schematic representations of NO adsorbed on Au_n (n = 1–3) clusters deposited on a O^{2-} site of the MgO(100) surface. a) Monomer; b) dimer; and c–d) trimers. Red spheres: O. Green spheres: Mg (including Mg-ECPs). Yellow spheres: Au. Grey spheres: N.

Table 4
Main energetic and electronic population parameters for NO adsorbed on Au particles deposited on a terrace site. NO stretching frequency (ν) and its shift with respect to free NO ($\Delta\nu$) are also shown.

	$NO/Au_1/MgO$	$NO/Au_2/MgO$	$NO/Au_3/MgO$	
			Fig. 6c	Fig. 6d
E_a (eV)	1.07	0.23	0.87	0.70
q[Au(1)] (e)	0.26	0.00	0.23	0.21
q[Au(2)]	–	0.00	0.13	−0.16
q[Au(3)]	–	–	−0.17	0.09
q(O)	−0.30	−0.20	−0.31	−0.30
q(N)	−0.07	0.07	−0.03	−0.02
q(NO)	−0.37	−0.13	−0.34	−0.32
SD[Au(1)]	–	0.05	–	–
SD[Au(2)]	–	0.00	–	–
SD[Au(3)]	–	–	–	–
SD(O)	–	0.32	–	–
SD(N)	–	0.61	–	–
ν_{NO} (cm^{-1})	1540	1716	1570	1594
$\Delta\nu_{NO}$	−336	−160	−306	−282

Table 5
Main energetic and electronic population parameters for NO adsorbed on Au particles deposited on an edge site. NO stretching frequency (ν) and its shift with respect to free NO ($\Delta\nu$) are also shown.

	$NO/Au_1/MgO$	$NO/Au_2/MgO$	$NO/Au_3/MgO$	
			Fig. 7c	Fig. 7d
E_a (eV)	1.06	0.22	0.82	0.32
q[Au(1)] (e)	0.27	0.03	0.26	0.27
q[Au(2)]	–	−0.01	0.03	0.21
q[Au(3)]	–	–	−0.02	−0.29
q(O)	−0.30	−0.21	−0.31	−0.26
q(N)	−0.08	0.05	−0.20	−0.09
q(NO)	−0.38	−0.16	−0.51	−0.36
SD[Au(1)]	–	0.03	–	–
SD[Au(2)]	–	0.00	–	–
SD[Au(3)]	–	–	–	–
SD(O)	–	0.21	–	–
SD(N)	–	0.62	–	–
ν_{NO} (cm^{-1})	1546	1714	1515	1593
$\Delta\nu_{NO}$	−330	−162	−361	−283

when this species is adsorbed isolated (see Fig. 7a). On the other hand, when NO adsorbs on the Au(2) atom, the triangle structure is preserved (Fig. 6d), but E_B is much lesser.

Finally in Fig. 8, the optimized geometries of the NO adsorption on Au_n/MgO for corner site are shown, and in Table 6 the main molecular parameters corresponding to these geometries. For Au_1 and Au_2, the NO adsorption on only one of the isoenergetic configurations previously shown in Fig. 4a and b (for Au_1/MgO) and in Fig. 4c and d (for Au_2/MgO) was considered. On the other hand, two different geometrical configurations are possible for the trimer. The N–O bond tilts with a Au–N–O angle of about 120°. In the trimer shown in Fig. 8c, the Au_3NO species adopts a conformation that is analogous to that of Fig. 6c (on terrace), but now the N atom is relatively near to a four-coordinated O^{2-}, with a $N–O_{4c}$ distance of 2.42 Å. In the second configuration, shown in Fig. 8d, NO molecule links to Au(3) atom of the trimer, weakening the Au(2)–Au(3) bond. In the resulting geometry, the Au_2 species is on the corner and the Au_1NO species is on the edge, with similar geometries than those of the same species but independently adsorbed.

For all the cases (terrace, edge and corner) the N–O distance for the adsorbed NO molecule is longer than calculated for the free molecule (1.158 Å). This stretching is higher for the monomer and trimer (0.03–0.05 Å longer) than that for the dimers (0.01–0.02 Å longer).

From the E_B values of Tables 4–6 we observe that the stabilization of NO on Au_n/MgO follows the order: $Au_1 > Au_3 \gg Au_2$. On the other hand, the Au–NO distance follows the order: $Au_2 > Au_3 > Au_1$, in line with the energetic sequence. In Fig. 9 the different values of E_B calculated for the adsorption of NO have been summarized together as a function of the number of Au atoms. For Au_3, the results for the most stable configurations were reported. An interesting feature is that the Au–NO interaction is rather insensitive to the topological site where the Au particle is anchored. A way of evaluating the effect of the support on the NO adsorption on Au is to compare the results for the $NO/Au_n/MgO$ systems with those of NO on free particles. In the latter case the binding energies are 0.73, 0.56 and 0.85 eV, for Au_1, Au_2 and Au_3, respectively (see Fig. 9). Therefore, the support acts favoring the adsorption in Au_1/MgO and disfavoring in Au_2/MgO. In Au_3/MgO the effect of the support is essentially neutral.

Both for terrace and topological defects, an electronic charge transfer takes place from the metal to the NO molecule, being more notorious on Au_1 and Au_3 where the charge of NO is in the range of −0.37/−0.46e and −0.32/−0.53e, respectively. On Au_2 it is much lower: −0.13/−0.22e. In the case of the free Au_nNO species, the charge of NO is considerably smaller: −0.06, −0.03 and −0.05e for Au_1NO, Au_2NO and Au_3NO, respectively. The latter results are very similar to those reported in Refs. [9] and [10], also using DFT. In general, the net charge of the adsorbed Au_nNO complexes is approximately the same than that of the adsorbed Au_n (Tables 1–3). Nevertheless, an internal electronic charge transference occurs from the Au_n particle to the NO molecule, being much higher for Au_1 and Au_3.

NO molecule adsorbs strongly on Au_1/MgO and Au_3/MgO, which are systems with an odd number of electrons and high SD in the metallic particle. In these cases, the NO molecule (a radical) strongly interacts with the Au particle through a covalent bond. For Au_2, a system with closed shell, the adsorption is much weaker. The same trend has been observed in recent calculations performed by Ding et al. [10] with DFT for the interaction of NO with very small Au particles at free state. Of all the particles analyzed (Au_1–Au_6), Au_1 and Au_3 present the highest NO adsorption energies; the Au–NO bond strength decreases monotonically, going from Au_4 to Au_6. Thus, Au_1 and Au_3, particles with an odd number of electrons, couple very efficiently with

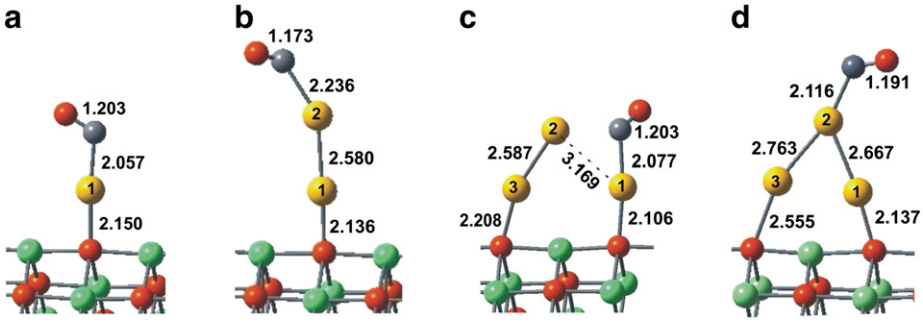

Fig. 7. Schematic representations of NO adsorbed on Au_n (n = 1–3) clusters deposited on a O^{2-} site of the edge topological defect of MgO. a) Monomer. b) Dimer. c)–d) Trimers. For the references to colors, see the figure legends of Fig. 6.

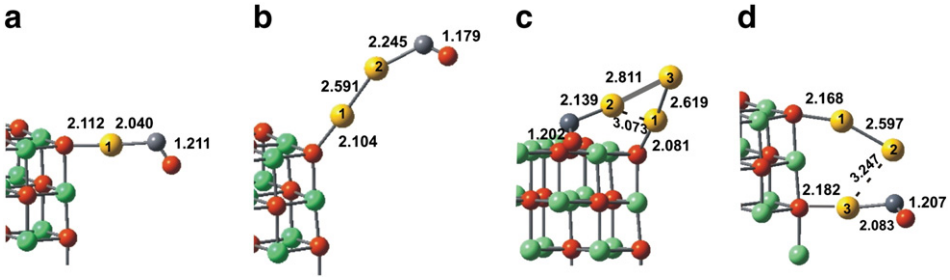

Fig. 8. Schematic representations of NO adsorbed on Au_n (n = 1–3) clusters deposited on a O^{2-} site of the corner topological defect of MgO. a) Monomer; b) dimer; and c–d) trimers. For the references to colors, see the figure legends of Fig. 6.

a radical as NO. Moreover the bonding takes place through the N atom because the SD is localized mainly on this atom in the NO molecule. Interestingly, Au_5 present a low capability to adsorb NO because the spin is highly diluted over the particle.

As it was mentioned above, the effect of the support is very different for Au_1 and Au_3. In previous works it was shown that in Au_1/MgO the spin is concentrated in a region above the Au atom [11,28] so that it becomes very reactive against radicals like NO. On the other hand, in Au_3 the spin is distributed over the whole particles both at free and supported states, and hence the support acts without modifying the NO–Au link. The relative high capability of supported Au_1 to interact with a radical like NO could be of great interest for experimentalists in order to design new materials capable to catalyze reactions involving NO and even to construct sensors for the detection of NO or other gases with similar open shell electronic structure.

With regard to the frequencies of N–O stretching reported in Tables 4–6 we notice that a red-shift of −330/−362, −160/−194 and −306/−390 cm^{-1} is predicted for NO adsorbed on Au_1/MgO, Au_2/MgO and Au_3/MgO, respectively, with respect to the frequency for isolated NO. The red-shift is much lower for Au_2, where the bonding between NO and the particle is weaker. From the $\Delta\nu$ values of Tables 4–6 we can observe that the red-shift is rather insensitive to the coordination of the O^{2-} site where the Au particle is anchored. The relative larger red-shift of NO adsorbed in Au_1/MgO and Au_3/MgO in comparison with that of Au_2/MgO can be related to the larger negative charge acquired by the NO molecule. As the electronic charge goes mainly to the $2\pi^*$ orbital of NO, which is antibonding, the N–O distance increases and the frequency decreases more significantly for Au_1/MgO and Au_3/MgO.

The system NO/Au/MgO has been experimentally studied by Solymosi et al. [2]. The peaks detected at 1718 cm^{-1} and 1697 cm^{-1} ($\Delta\nu_{NO}$ = −158 cm^{-1} and −179 cm^{-1}, respectively) were assigned to $AuNO^-$ species. Nevertheless, these results are not in principle comparable with ours since the Au particle size in these catalysts is large, with a dispersion of about 7%. On the other hand, for the NO/Au/TiO_2 system, Debeila et al. [44] found a larger red-shift of −222 cm^{-1}. The authors suggested that this shift is due to the interaction of NO with the Au–TiO_2 interface and/or to the adsorption on Au particles in the vicinities of O-vacancies. Unfortunately, no experimental works devoted to the adsorption of NO on tiny supported Au particles have been published yet. However, recently Sterrer et al. [22] performed UHV experiments on the CO adsorption on MgO-supported Au atoms, finding a significant red-shift of −291 cm^{-1} for C–O stretching, far below of other values reported for gold-based systems.

Table 6
Main energetic and electronic population parameters for NO adsorbed on Au particles deposited on a corner site. NO stretching frequency (ν) and its shift with respect to free NO ($\Delta\nu$) are also shown.

	NO/Au_1/MgO	NO/Au_2/MgO	NO/Au_3/MgO	
			Fig. 8c	Fig. 8d
E_a (eV)	1.19	0.22	0.82	0.86
q[Au(1)] (e)	0.32	0.31	0.30	0.08
q[Au(2)]	–	−0.07	−0.23	−0.04
q[Au(3)]	–	–	0.11	0.25
q(O)	−0.34	−0.25	−0.34	−0.33
q(N)	−0.12	0.03	−0.11	−0.20
q(NO)	−0.46	−0.22	−0.47	−0.53
SD[Au(1)]	–	0.00	–	–
SD[Au(2)]	–	0.00	–	–
SD[Au(3)]	–	–	–	–
SD(O)	–	0.34	–	–
SD(N)	–	0.65	–	–
ν_{NO} (cm^{-1})	1514	1682	1517	1486
$\Delta\nu_{NO}$	−362	−194	−359	−390

4. Conclusions

The main conclusions of the present work can be summarized as follows:

- The adhesion of gold is greater for Au_2 and Au_3 than for Au_1, being the interaction of polarization type.
- The reactivity of these Au particles in relation to NO adsorption can be explained considering the electronic configuration of Au_n/MgO systems. Open shell systems as Au_1/MgO and Au_3/MgO are very reactive while Au_2/MgO, with a close shell structure, is poorly reactive.
- Comparing with the interaction of NO with free Au particles, the MgO support enhances the NO–Au_n bonding strength in the case of monomers, weakens this bond in the case of dimers and does not have an effect in the trimers. In this comparison, the increases of the NO binding energy for Au_1, by going from isolated to supported Au particles, are 0.34, 0.33 and 0.46 eV for terrace, edge and corner,

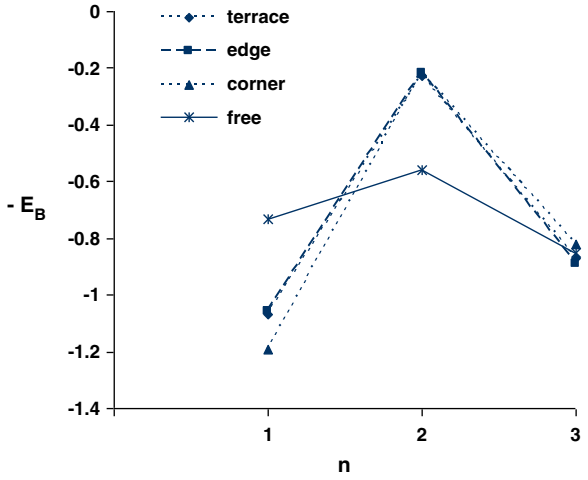

Fig. 9. Binding energy (E_B, in eV) of NO molecule vs. the number of atoms in Au_n particles. For the trimers, only the result for the most stable structure is reported.

respectively. In Au_3, the dilution of the spin on both free and supported states can explain the slight effect of the support. In the case of monomer, supported Au_1 is more reactive than the free species because, by the effect of the support, the spin concentrates in a region above the Au atom making it very reactive against a radical like NO.

- The adsorbed NO–Au_n species has nearly the same net charge than that of the Au_n particle before adsorption. However, an internal Au → NO electronic transfer is produced.
- The N–O stretching frequency shows a significant red-shift, from -300 to $-390\ cm^{-1}$ in the case of Au_1/MgO and Au_3/MgO, and in the range $-160/-190\ cm^{-1}$ in the case of Au_2/MgO. These shifts correlate with the amount of negative charge of NO.
- The NO–Au_n bonding is relatively insensitive to the coordination of the anionic site where the Au_n particle is anchored. Nevertheless, and particularly for the trimers, different geometrical configurations for the NO–Au_n species are possible.

Acknowledgments

The authors acknowledge the financial support of Universidad Nacional del Sur, CONICET and ANPCyT of Argentina.

References

[1] M. Haruta, Catal. Today 36 (1997) 153.
[2] F. Solymosi, T. Bánsági, T.S. Zakar, Phys. Chem. Chem. Phys. 5 (2003) 4724.
[3] K. Blick, T.D. Mitrelias, J.S.J. Hargreaves, G.J. Hutchings, R.W. Joyner, C.J. Kiely, F.E. Wagner, Catal. Lett. 50 (1998) 211.
[4] A. Ueda, M. Haruta, Gold Bull. 32 (1) (1999) 3.
[5] W.A. Brown, D.A. King, J. Phys. Chem. B 104 (2000) 2578.
[6] H. Over, Prog. Surf. Sci. 58 (2001) 249.
[7] S. Roy, M.S. Hedge, G. Madras, Appl. Energy 86 (2009) 2283.
[8] Y. Hu, K. Griffiths, P.R. Norton, Surf. Sci. 603 (2009) 1740.
[9] A. Citra, X. Wang, L. Andrews, J. Phys. Chem. A 106 (2002) 3287.
[10] X. Ding, Z. Li, J. Yang, J.G. Hou, Q. Zhu, J. Chem. Phys. 121 (2004) 2558.
[11] A. Del Vitto, G. Pacchioni, F. Delbecq, P. Sautet, J. Phys. Chem. B 109 (2005) 8040.
[12] L.M. Molina, J.A. Alonso, J. Phys. Chem. C 111 (2007) 6668.
[13] G. Barcaro, A. Fortunelli, J. Chem. Theory Comput. 1 (2005) 972.
[14] P. Frondelius, H. Häkkinen, K. Honkala, New J. Phys. 9 (2007) 339.
[15] P. Frondelius, H. Häkkinen, K. Honkala, Phys. Rev. B 76 (2007) 073406.
[16] L.M. Molina, B. Hammer, Phys. Rev. B 69 (2004) 155424.
[17] R. Caballero, C. Quintanar, A.M. Köster, S.N. Khanna, J.U. Reveles, J. Phys. Chem. C 112 (2008) 14919.
[18] A. Bogicevic, D.R. Jennison, Surf. Sci. 515 (2002) L481.
[19] C. Inntam, L.V. Moskaleva, K.M. Neyman, V.A. Nasluzov, N. Rösch, Appl. Phys. A 82 (2006) 181.
[20] H. Grönbeck, P. Broqvist, J. Chem. Phys. B 107 (2003) 12239.
[21] R.M. Ferullo, S.A. Fuente, P.G. Belelli, N.J. Castellani, Surf. Sci. 603 (2009) 1262.
[22] M. Sterrer, M. Yulikov, T. Risse, H.J. Freund, J. Carrasco, F. Illas, C. Di Valentin, L. Giordano, G. Pacchioni, Angew. Chem. Int. Ed. 45 (2006) 2633.
[23] L. Giordano, J. Carrasco, C. Di Valentin, F. Illas, G. Pacchioni, J. Chem. Phys. 124 (2006) 174709.
[24] A. Sanchez, S. Abbet, U. Heiz, W.-D. Schneider, H.H. Häkkinen, R.N. Barnett, U. Landman, J. Phys. Chem. A 103 (1999) 9573.
[25] L.M. Molina, B. Hammer, Phys. Rev. Lett. 90 (2003) 206102.
[26] B. Yoon, H. Häkkinen, U. Landman, A.S. Wörz, J.-M. Antonietti, S. Abbet, K. Judai, U. Heiz, Science 307 (2005) 403.
[27] C. Zhang, B. Yoon, U. Landman, J. Am. Chem. Soc. 129 (2007) 2228.
[28] S.A. Fuente, P.G. Belelli, R.M. Ferullo, N.J. Castellani, Surf. Sci. 602 (2008) 1669.
[29] A.D. Becke, J. Chem. Phys. 98 (1993) 5648.
[30] M.J. Frisch, et al., Gaussian 03, Revision C.02, Gaussian, Inc., Wallingford, CT, 2004.
[31] J. Carrasco, C. Sousa, F. Illas, P.V. Sushko, A.L. Shluger, J. Chem. Phys. 125 (2006) 074710.
[32] J. Carrasco, N. Lopez, F. Illas, H.-J. Freund, J. Chem. Phys. 125 (2006) 074711.
[33] L. Giordano, J. Carrasco, C. Di Valentin, F. Illas, G. Pacchioni, J. Chem. Phys. 124 (2006) 174709.
[34] P.J. Hay, W.R. Wadt, J. Chem. Phys. 82 (1985) 270.
[35] P.J. Hay, W.R. Wadt, J. Chem. Phys. 82 (1985) 299.
[36] I. Yudanov, G. Pacchioni, K. Neyman, N. Rösch, J. Phys. Chem. B 101 (1997) 2786.
[37] S.F. Boys, F. Bernardi, Mol. Phys. 19 (1970) 553.
[38] A.E. Reed, L.A. Curtiss, F. Weinhold, Chem. Rev. 88 (1988) 899.
[39] J. Zhou, F. Xiao, W.-N. Wang, K.-N. Fan, J. Mol. Struct. THEOCHEM 818 (2007) 51.
[40] S. Jiang, S. Huang, W. Tu, J. Zhu, Appl. Surf. Sci. 255 (2009) 5764.
[41] S.A. Fuente, P.G. Belelli, M.M. Branda, R.M. Ferullo, N.J. Castellani, Appl. Surf. Sci. 255 (2009) 7380.
[42] H.J. Freund, Catal. Today 117 (2006) 6.
[43] G. Barcaro, A. Fortunelli, New J. Phys. 9 (2007) 22.
[44] M.A. Debeila, N.J. Coville, M.S. Scurrell, G.R. Hearne, J. Mol. Catal. A 219 (2004) 131.